J|A|C|S
ARTICLES
Published on Web 10/12/2002

Synthesis, Characterization, and Catalytic Performance of Single-Site Iron(III) Centers on the Surface of SBA-15 Silica

Chika Nozaki,[†,‡] Claus G. Lugmair,[†,‡] Alexis T. Bell,*[,§,‡] and T. Don Tilley*[,†,‡]

Contribution from Department of Chemistry and Department of Chemical Engineering, University of California, Berkeley, Berkeley, California 94720-1460, and Chemical Sciences Division, Lawrence Berkeley National Laboratory, 1 Cyclotron Road, Berkeley, California 94720

Received March 15, 2002

Abstract: A new molecular precursor strategy has been used to prepare a series of single-site catalysts that possess isolated iron centers supported on mesoporous SBA-15 silica. The iron centers were introduced via grafting reactions of the tris(*tert*-butoxy)siloxy iron(III) complex $Fe[OSi(O^tBu)_3]_3(THF)$ with SBA-15 in dry hexane. This complex reacts cleanly with the hydroxyl groups of SBA-15 to eliminate $HOSi(O^tBu)_3$ (as moniored by ^1H NMR spectroscopy) with formation of isolated surface species of the type $\equiv SiO-Fe-[OSi(O^tBu)_3]_2(THF)$. In this way, up to 21% of the hydroxyl sites on SBA-15 were derivatized (0.23 Fe nm^{-2}), and iron loadings in the range of 0.0−1.90% were achieved. The structure of the surface-bound iron species, as determined by spectroscopic methods (electron paramagnetic resonance (EPR), nuclear magnetic resonance (NMR), UV−vis, and in situ infrared measurements) and by elemental analyses, contains a pseudotetrahedral iron(III) center. The THF ligand of this surface-bound complex was quantitatively displaced by acetonitrile (by ^1H NMR spectroscopy). Calcination of these materials at 300 °C for 2 h under oxygen resulted in removal of all organic matter and site-isolated iron surface species that are stable to condensation to iron oxide clusters. Spectroscopic data (UV−vis and EPR) suggest that the iron centers retain a mononuclear, pseudotetrahedral iron(III) structure after calcination. The calcinated, iron-grafted SBA-15 materials exhibit high selectivities as catalysts for oxidations of alkanes, alkenes, and arenes, with hydrogen peroxide as the oxidant.

Introduction

Important goals in heterogeneous catalysis include the characterization, design, and synthesis of active and selective catalytic centers. Progress in this direction will rely on establishment of structure−reactivity relationships via structural and mechanistic studies, but this is particularly challenging for heterogeneous catalysts given the inherent difficulty in characterizing active sites under reaction conditions.[1,2] For many catalysts, it is apparent that desirable properties are associated with well-defined active sites containing one or only a few metal centers on the surface of a support.[3−6] Thus, it is important to develop methods for the controlled, chemical modification of surfaces with introduction of precisely defined inorganic species. Most attempts to introduce surface-bound active sites have centered on aqueous impregnation methods. However, this technique is somewhat limited by the tendency of many metal-based species to agglomerate on the surface of the support during dehydration.[7]

The iron-containing zeolite FeZSM-5 has attracted considerable attention due to its high activity as a catalyst for the reduction of nitrogen oxides (NO_x),[8] and for the selective oxidation of hydrocarbons with nitrous oxide as the oxidant.[9,10] Given the potential utility of this catalyst, several investigations have sought to determine the state of iron in FeZSM-5 and the structure of the active site. Lobree et al.[11] have reported that at iron loadings below Fe/Al = 0.56 the iron is in the form of isolated cations displacing a fraction of the Brønsted acid sites. Marturano et al.[12] report that *di*ferric oxo-bridged clusters form within the silicoalumina framework. On the other hand, Joyner and Stockenhuber[13] have proposed an Fe_4O_4 nanocluster as a

* Address correpondence to this author. E-mail: tdtilly@socrates.berkeley.edu.
† Department of Chemistry.
§ Department of Chemical Engineering.
‡ Lawrence Berkeley National Laboratory.

(1) Le Page, J.-F.; Cosyns, J.; Courty, P.; Freund, E.; Franck, J.-P.; Jacquin, Y.; Juguin, B.; Marcilly, C.; Martino, G.; Miquel, J.; Montanal, R.; Sugier, A.; van Landeghem, H. In *Applied Heterogeneous Catalysis*; Limido, J., Ed.; Editions Technip: Paris, 1987.
(2) Wachs, I. E.; Deo, G.; Jehng, J.-M.; Kim, D. S.; Hu, H. In *Heterogeneous Hydrocarbon Oxidation*; Warren, B. K., Oyama, S. T., Eds.; ACS symposium Series 638; American Chemical Society: Washington, DC, 1996; pp 292−299.
(3) Thomas, J. M. *Top. Catal.* **2001**, *15*, 85−92.
(4) Grasselli, R. K. *Top. Catal.* **2001**, *15*, 93−102.
(5) Volta, J.-C. *Top. Catal.* **2001**, *15*, 121−130.
(6) Millet, J.-M. M.; Védrine, J. C. *Top. Catal.* **2001**, *15*, 139−144.
(7) Ratnasamy, P.; Kumar, R. *Catal. Today* **1991**, *9*, 328−416.
(8) Chen, H.-Y.; Sachtler, W. M. H. *Catal. Today* **1998**, *42*, 73−83.
(9) Panov, G. I.; Uriaete, A. K.; Rodkim, M. A.; Sobolov, V. I. *Catal. Today* **1998**, *41*, 365−385.
(10) Sobolev, V. I.; Dubkov, K. A.; Panna, O. V.; Panov, G. I. *Catal. Today* **1995**, *24*, 251−252.
(11) Lobree, L. J.; Hwang, I.-C.; Reimer, J. A.; Bell, A. T. *J. Catal.* **1999**, *186*, 242−253.
(12) Marturano, P.; Drozdová, L.; Kogelbauer, A.; Prins, R. *J. Catal.* **2000**, *192*, 236−247.
(13) Joyner, R.; Stockenhuber, M. *J. Phys. Chem. B* **1999**, *103*, 5963−5976.

10.1021/ja020388t CCC: $22.00

possible state of iron in FeZSM-5. Although there is no consensus on the nature of the iron centers, it seems clear that some type of isolated iron site plays an important role in the selective processes catalyzed by FeZSM-5.

Given the increasing interest in the structure and catalytic chemistry of supported iron centers, we have attempted to develop reliable routes to stable, well-defined inorganic iron species bound to an oxide support. Herein, we describe a process for the introduction of isolated, tetrahedral iron(III) centers onto a silica surface, involving grafting reactions with molecular precursors. This method produces iron sites that are remarkably stable with respect to thermal degradation to iron oxide clusters. Previous reports have described attempts to synthesize iron-supported silica materials from inorganic iron species such as $FeCl_3$,[14,15] $FePO_4$,[16] and $Fe_2(SO_4)_3 \cdot 7H_2O$.[17] In general, these procedures do not produce stable, isolated iron surface species, as the aqueous media and calcination treatments lead to condensation of the iron into iron oxide clusters.

Other efforts to prepare catalytic, supported iron species have involved the grafting of molecular iron complexes onto silica via an organic "tether". Many of the resulting heterogeneous catalysts have been inspired by iron-containing enzymes (especially cytochrome P-450 and methane monooxygenase),[18−24] and involve grafting of biomimetic iron model complexes[25−36] onto silica. For example, tetrakis(pentafluorophenyl)porphyrin iron(II) has been grafted onto silica gel modified with 1,6-diaminohexane,[33] and $[Fe_2O(\eta^1-H_2O)(\eta^1-OAc)(TPA)_2]^{3+}$ (TPA = tris[(2-pyridyl)methyl]amine) may be incorporated into silica modified with poly(ethylene oxide) and poly(propylene oxide).[34] Molecular iron species have also been attached to the surface of an MCM-41 silica material via the linker 3-aminopropyltrimethoxysilane,[35] and iron porphyrin species have been incorporated into MCM-41.[36]

Scheme 1

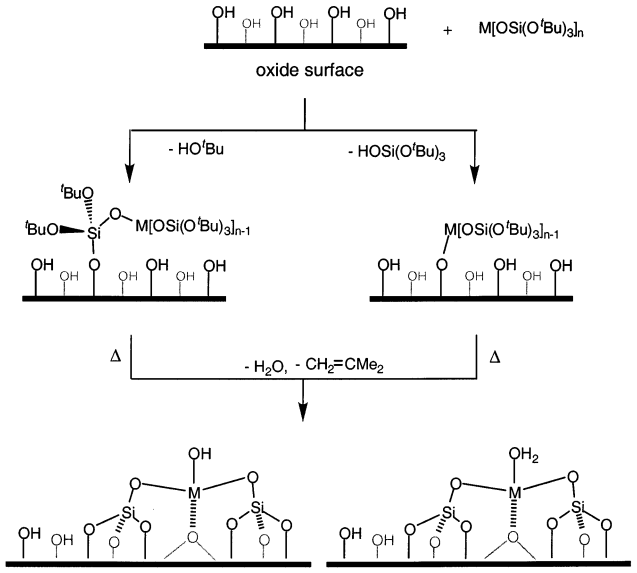

As discussed elsewhere, we have shown that the thermolytic molecular precursor route to oxide materials[37−45] may also be used to introduce catalytic titanium sites onto the surface of a silica support.[46,47] A potential advantage to this approach is that it may allow molecular-level control over the structure of the catalytic site, as illustrated in the generalized (hypothetical) transformations shown in Scheme 1. Initially, the precursor molecule is bonded to the surface via protonolysis reactions, which in the case of a precursor of the type $M[OSi(O^tBu)_3]_n$, may occur with loss of HO^tBu or $HOSi(O^tBu)_3$. Depending on this grafting chemistry, the species bound to the surface will be attached via M−O−(surface) or Si−O−(surface) linkages, respectively. Calcination should then lead to loss of the organic fragments of the immobilized species, in a manner similar to that observed for the "bulk transformations", to produce isolated $MO_x \cdot (n-1)SiO_2$ species on the oxide surface. The new site may be partially supported by the few equivalents of silica that are introduced by the molecular precursor, and in this way, stabilized. The goals of the work described here are to determine whether this method is effective for the introduction of stable, single-iron sites on silica and to characterize the properties of such species as catalysts for selective hydrocarbon oxidations. For this purpose, the iron precursor $Fe[OSi(O^tBu)_3]_3(THF)$ has been employed. As the oxide support, we have chosen SBA-15[48] as it possesses a high surface area and hydroxyl groups on

(14) Schuchardt, U.; Pereira, R.; Krahembuhl, C. E. Z.; Pufo, M.; Buffon, R. *Appl. Catal.* **1995**, *131*, 135−141.
(15) Tagawa, T.; Seo, Y.; Goto, S. *J. Mol. Catal.* **1993**, *78*, 201−210.
(16) McCormick, R. L.; Alptekin, G. O.; Williamson, D. L.; Ohno, T. R. *Top. Catal.* **2000**, *10*, 115−122.
(17) Kurusu, Y.; Neckers, D. C. *J. Org. Chem.* **1991**, *56*, 1981−1983.
(18) *Cytochrome P450;* Ortiz de Montellano, P. R., Ed.; Plenum: New York, 1986.
(19) Fontecave, M.; Ménage, S.; Duboc-Toia, C. *Coord. Chem. Rev.* **1998**, *178−80*, 1555−1572.
(20) Rosenzweig, A. C.; Frederick, C. A.; Lippard. S. J.; Nordlund, P. *Nature* **1993**, *366*, 537−543.
(21) Feig, A.; Lippard, S. J. *Chem. Rev.* **1994**, *96*, 759−805.
(22) Rosenzweig, A. C.; Nordlund, P.; Takahara, P. M.; Frederick, C. A.; Lippard, S. J. *Chem. Biol.* **1995**, *2*, 409−418.
(23) Holm, R. H.; Kennepohl, P.; Solomon, E. I. *Chem. Rev.* **1996**, *96*, 2239−2314.
(24) Solomon, E. I.; Brunold, T. C.; Davis, M. I.; Kemsley, J. N.; Lee, S.-K.; Lehnert, N.; Neese, F.; Skulan, A. J.; Yang, Y.-S.; Zhou, J. *Chem. Rev.* **2000**, *100*, 235−349.
(25) Costas, M.; Pohde, J.-U.; Stubna, A.; Ho, R. Y. N.; Quaroni, L.; Münck, E.; Que, L., Jr. *J. Am. Chem. Soc.* **2001**, *123*, 12931−12932.
(26) Chen, K.; Que, L., Jr. *J. Am. Chem. Soc.* **2001**, *123*, 6327−6337.
(27) Dolphin, D.; Traylor, T. G.; Xie, L. Y. *Acc. Chem. Res.* **1997**, *30*, 251−259.
(28) *Metalloporphyrins in Catalytic Oxidations;* Sheldon, R. A., Ed.; Marcel-Dekker: New York, 1994.
(29) MacBeth, C. E.; Golombek, A. P.; Young, V. G.; Yang, C.; Kuczera, K.; Hendrich, M. P.; Borovik, A. S. *Science* **2000**, *289*, 938−941.
(30) Grinstaff, M. W.; Hill, M. G.; Labinger, J. A.; Gray, H. B. *Science* **1994**, *264*, 1311−1313.
(31) White, M. C.; Doyle, A.; Jacobsen, E. N. *J. Am. Chem. Soc.* **2001**, *123*, 7194−7195.
(32) Lee, D.; Lippard, S. J. *Inorg. Chem.* **2002**, *41*, 827−837.
(33) Evans, S.; Smith, J. R. L. *J. Chem. Soc., Perkin Trans. 2* **2001**, *2*, 174−180.
(34) Neimann, K.; Neumann, R.; Rabion, A.; Buchanan, R. M.; Fish, R. H. *Inorg. Chem.* **1999**, *38*, 3575−3580.
(35) Carvalho, W. A.; Wallau, M.; Schuchardt, U. *J. Mol. Catal. A: Chem.* **1999**, *144*, 91−99.
(36) Schunemann, V.; Trautwein, A. X.; Rietjens, I. M. C. M.; Boersma, M. G.; Veeger, C.; Mandon, D.; Weiss, R.; Bahl, K.; Colapietro, C.; Piech, M.; Austin, R. N. *Inorg. Chem.* **1999**, *38*, 4901−4905.
(37) Terry, K. W.; Tilley, T. D. *Chem. Mater.* **1991**, *3*, 1001−1003.
(38) Terry, K. W.; Lugmair, C. G.; Gantzel, P. K.; Tilley, T. D. *Chem. Mater.* **1996**, *8*, 274−280.
(39) Su, K.; Tilley, T. D. *Chem. Mater.* **1997**, *9*, 588−595.
(40) Su, K.; Tilley, T. D.; Sailor, M. J. *J. Am. Chem. Soc.* **1996**, *118*, 3459−3468.
(41) Terry, K. W.; Lugmair, C. G.; Tilley, T. D. *J. Am. Chem. Soc.* **1997**, *119*, 9745−9756.
(42) Coles, M. P.; Lugmair, C. G.; Terry, K. W.; Tilley, T. D. *Chem. Mater.* **2000**, *12*, 122−131.
(43) Rulkens, R.; Male, J. L.; Terry, K. W.; Olthof, B.; Khodakov, A.; Bell, A. T.; Iglesia, E.; Tilley, T. D. *Chem. Mater.* **1999**, *11*, 2966−2973.
(44) Kriesel, J. W.; Sander, M. S.; Tilley, T. D. *Adv. Mater.* **2001**, *13*, 331−335.
(45) Fujdala, K. L.; Tilley, T. D. *J. Am. Chem. Soc.* **2001**, *123*, 10133−10134.
(46) Jarupatrakorn, J.; Tilley, T. D. *J. Am. Chem. Soc.* **2002**, *124*, 8380-8388.
(47) Tilley, T. D. *J. Mol. Catal. A: Chem.* **2002**, *182−183*, 17.
(48) Zhao, D.; Huo, Q.; Feng, J.; Chemelka, B. F.; Stucky, G. D. *J. Am. Chem. Soc.* **1998**, *120*, 6024−6036.

the surface. The resulting materials are catalysts for selective oxidations of alkanes, alkenes, and aromatic compounds with hydrogen peroxide as the oxidant.

Experimental Section

All synthetic manipulations were performed under an atmosphere of argon or nitrogen using standard Schlenk techniques and/or in a Vacuum Atmospheres drybox. Tri(*tert*-butoxy)silanol[49] and the sodium salt of tri(*tert*-butoxyl)silanol[50] were prepared according to literature procedures. ^{1}H NMR spectra were recorded on a Bruker AMX 400 spectrometer (400 MHz), or on a GE QE-300 instrument (at 300 MHz). Specific surface areas were measured using the BET method on a Quantachrome surface area analyzer. Powder X-ray diffraction was performed on a Siemens D 5000 diffractometer (Cu Kα, $\lambda = 0.15406$ nm, 45 kV, 35 mA). Elemental analyses were performed at Mikroanalytiches Labor Pascher, at Desert Analytics, or at the UC Berkeley College of Chemistry Microanalytical Facility. Diffuse reflectance UV−vis spectra were recorded using a Varian−Cary 4 spectrophotometer equipped with a Harrick diffuse-reflectance attachment. MgO was used as a reference. UV−vis measurements in solution were performed on a Hewlett-Packard 89532A diode array spectrophotometer with HP operating software. X-band electron paramagnetic resonance (EPR) measurements were made at room temperature using a Bruker EMX EPR spectrometer. All EPR samples were handled under nitrogen. The grafting reactions were monitored by ^{1}H NMR spectroscopy, employing J-Young NMR tubes to maintain an anhydrous, nitrogen atomosphere. Ferrocene was used as an internal standard. The grafting reaction was initiated by adding SBA-15 to an excess of Fe[OSi(O^{t}Bu)$_3$]$_3$(THF) in benzene-d_6 at room temperature. The ligand-exchange reaction was initiated by adding excess dry CH_3CN to an iron-grafted SBA-15 sample (with 1.90 wt % Fe) suspended in benzene-d_6 at room temperature. Thermal analyses were performed on a DuPont model 2000 thermal analysis system. In situ infrared spectra were recorded using a Nicolet Nexus 670 FT-IR instrument with a MCT-A detector. Measurements were made at a resolution of 4 cm^{-1} with a total of 64 scans per spectrum. Total gas flow rates for all experiments were 60 mL/min. Samples were pressed into 30-mg self-supporting pellets, which were placed into an IR cell. CaF_2 IR windows were used. The sample was heated from 25 to 500 °C at a rate of 5 °C/min under oxygen. The IR spectra were monitored at 50 °C intervals. SBA-15 was used as a background. The background spectrum of SBA-15 was subtracted to obtain spectra of target samples consisting of only absorbances due to adsorbed species. The number of hydroxyl groups on SBA-15 was measured by ^{1}H NMR spectroscopy, using $Mg(CH_2Ph)_2$ according to a literature procedure.[45] GC analyses were performed with a Hewlet Packard HP 6890 series GC system using a methylsiloxane capillary (50.0 m × 320 μm × 1.05 μm nominal), and integration was performed relative to an internal standard (dodecane).

Fe[OSi(O^{t}Bu)$_3$]$_3$(THF).[51] A THF (20 mL) solution of (*tert*-BuO)$_3$SiONa (1.07 g, 4.0 mmol) was added to a stirred THF (20 mL) solution of $FeCl_3$ (0.216 g, 1.33 mmol). The reaction mixture was refluxed for 14 h. The solvent was removed under reduced pressure, and the resulting solid was extracted into pentane (40 mL). Concentration and cooling (−40 °C) of the pentane solution afforded yellow crystals, and two subsequent recrystallizations produced the pure compound in 74% yield (0.82 g). Anal. Calcd for $C_{40}H_{89}O_{13}Si_3Fe_1$: C, 52.32; H, 9.77. Found: C, 52.17; H, 9.81. IR (Nujol, CsI, cm^{-1}): 1364s, 1242m, 1212vw sh, 1190s, 1055s, 1026s, 985s, 912w, 828m, 803w, 702m, 648w, 536w sh, 517w sh, 495w, 479w sh, 472w sh, 433w. ^{1}H NMR (benzene-d_6, 22 °C, ppm): no peaks observed. UV−vis in hexane: 37594 cm^{-1} ($\epsilon = 2388$ M^{-1} cm^{-1} in 4.50×10^{-5} M solution), 22124 cm^{-1} ($\epsilon = 11$ M^{-1} cm^{-1} in 6.60×10^{-3} M solution).

(49) Abe, Y.; Kijima, I. *Bull. Chem. Soc. Jpn.* **1969**, *42*, 1118−1123.
(50) McMullen, A. K.; Tilley, T. D.; Rheingold, A. L.; Geib, S. J. *Inorg. Chem.* **1989**, *28*, 3772−3774.
(51) Lugmair, C. G. Ph.D. Thesis, University of California, Berkeley, CA, 1997.

Table 1. Crystallographic Data for Fe[OSi(O^{t}Bu)$_3$]$_3$(THF)

crystal parameters	
formula	$C_{40}H_{89}FeO_{14}Si_3$
formula weight	934.24
cryst color, habit	yellow, blocky
crystal size, mm	0.40 × 0.25 × 0.15
crystal system	monoclinic
space group	$P2_1/c$
a, Å	25.7175(3)
b, Å	18.2111(2)
c, Å	26.5506(3)
β, deg	95.349(1)
volume, Å^3	11010.7(3)
Z	8
ρ (calcd), g cm^{-3}	1.127
μ (Mo Kα), cm^{-1}	3.91
temp, °C	-102
data collection	
diffractometer	Siemens SMART
radiation	MoKα ($\lambda = 0.71073$ Å)
scan type	ω(0.3 ° per frame)
rflns. collected	45137
unique rflns.	16240 ($R_{int} = 0.051$)
no. observations	8581 ($I > 3.00\sigma(I)$)
refinement	
rfln./param ratio	8.69
R(F), %	9.1
R(wF), %	10.9
GOF	3.55
max/min peak in final diff map, eÅ^{-3}	0.92; −0.57

Crystallographic Structure Determination of Fe[OSi(O^{t}Bu)$_3$]$_3$(THF). Crystal, data collection, and refinement parameters are collected in Table 1. Crystals of Fe[OSi(O^{t}Bu)$_3$]$_3$(THF) were grown from a concentrated pentane solution at −80 °C. A slightly yellow, blocky crystal of dimensions 0.40mm × 0.25mm × 0.15 mm was mounted on a glass fiber using Paratone N hydrocarbon oil. Data were collected using a Siemens SMART diffractometer with a CCD area detector. A preliminary orientation matrix and unit cell parameters were determined by collecting 60 10-s frames, followed by spot integration and least-squares refinement. A hemisphere of data was collected using ω scans of 0.3° and a collection time of 30 s per frame. Frame data were integrated (*XY* spot spread = 1.60°; *Z* spot spread = 0.60°) using SAINT. The data were corrected for Lorentz and polarization effects. An adsorption correction was performed using XPREP (μR = 0.06, $T_{max} = 0.93$, $T_{min} = 0.88$). The 45 137 integrated reflections were averaged in point group 2/m to give 16 240 unique reflections ($R_{int} = 0.051$). Of these, 8581 reflections were considered observed ($I > 3.00\sigma(I)$). No decay correction was necessary. Inspection of the systematic absences uniquely defined the space group as $P2_1/c$. The structure was solved using direct methods (SIR92), expanded using Fourier techniques (DIRDIF92), and refined by full matrix least-squares methods using teXsan software. The atoms that were modeled as disordered over two sites were refined isotropically. The pairs of disordered atoms O(3)−O(4), O(5)−O(6), O(16)−O(17), O(18)−O(19), O(30)−O(31), O(32)−O(33), C(12)−C(13), C(17)−C(18), C(44)−C(45), C(46)−C(47), C(48)−C(49), C(50)−C(51), C(55)−C(56), C(58)−C(59), C(62)−C(63), C(80)−C(81), C(91)−C(92), and C(109)−C(110) were refined with equal populations. The pairs of disordered atoms O(20)−O(21), O(22)−O(23), C(10)−C(11), C(22)−C(23), C(66)−C(65), C(68)−C(67), C(70)−C(69), C(78)−C(79), C(87)−C(88), C(89)−C(90), C(95)−C(94), and C(97)−C(96) were refined with 60 and 40% relative populations, respectively. The pairs of disordered atoms C(2)−C(3), C(4)−C(5), C(6)−C(7), C(61)−C(60), C(76)−C(77), C(99)−(98), C(102)−C(101), C(104)−C(103), and C(106)−C(105) were refined with 70 and 30% relative populations, respectively. The remaining atoms were refined anisotropically. No hydrogen atoms were included in the model. The number of variable parameters was 988, giving a

Table 2. Iron Content of Materials Prepared by Room Temperature Grafting of $Fe[OSi(O^tBu)_3]_3(THF)$ onto SBA-15

Fe/wt %	Fe/nm^2 *a*	Fe/≡SiOH *b*
0.056	6.8×10^{-3}	0.0063
0.35	0.042	0.039
0.50	0.061	0.057
1.33	0.16	0.15
1.90 (max loading)	0.23	0.21

a Calculated on the basis of the surface area of SBA-15: 875 m^2/g. *b* Calculated on the basis of the number of surface hydroxyl groups on silica measured by ^{1}H NMR spectroscopy: 1.07 OH groups/nm^2.

data parameter ratio of 8.69. The maximum and minimum peaks on the final difference Fourier map corresponded to 0.92 and −0.57 e$^-$Å^{-3}: $R = 0.091$, $R_w = 0.109$, GOF = 3.55.

SBA-15.[48] Four grams of P123 ($EO_{20}PO_{70}EO_{20}$) was dissolved in 30 g of deionized water and 120 g of 2 M HCl solution, with stirring. Then, 9.1 mL of tetraethoxysilane (TEOS) was added to the solution, and the resulting mixture was stirred at room temperature for 20 h. The solid product was recovered, washed, and air-dried at room temperature. The solid was calcined at 550 °C for 10 h and then dried at 190 °C under nitrogen for 12 h. The yield was 95% (based on silicon). X-ray diffraction analysis: Main three peaks at $2\theta = 1.234°$ ($d_{100} =$ 71.5 Å), 1.836° ($d_{110} = 48.1$ Å), and 3.313° ($d_{200} = 26.6$ Å) with an intensity ratio of 81/8/11. BET surface area: 875 m^2 g^{-1}. Total pore volume: 0.92 cm^3/g. Pore diameter: 66 Å. Anal. Found: C, 0.2%; H, 0.3%. The OH coverage was 1.07 OH/nm^2, as determined by monitoring the reaction with $Mg(CH_2Ph)_2$ by ^{1}H NMR spectroscopy.[45]

Grafting $Fe[OSi(O^tBu)_3]_3$(THF) Onto Mesoporous Silica. SBA-15 (0.5 g) was suspended in dry hexane (25 mL) for 2 h under nitrogen. $Fe[OSi(O^tBu)_3]_3$(THF) (for 0.056−1.90% Fe loadings, 0.00461−0.157 g; 0.0050−0.17 mmol) was dissolved in dry hexane (25 mL), and this solution was then added to the suspension of SBA-15. The resulting mixture was stirred at room temperature for 24 h. The solid product was collected, washed with dry hexane (3 × 20 mL), and then dried under reduced pressure. The product was calcined at 300 °C under dry oxygen for 2 h. The loadings of Fe were 0.056, 0.35, 0.50, 1.33, and 1.90 wt % Fe as shown in Table 2. The [Fe]/[≡SiOH] ratios were calculated on the basis of the number of surface hydroxyl groups on silica, 1.07 OH groups/nm^2.

Catalytic Oxidations. A sample of the catalyst (130 mg) was added to a 50-mL round-bottom flask that had previously been evacuated and filled with nitrogen three times. Substrates (18.5−22.4 mmol), acetonitrile (5 mL), and dodecane (428 μmol) were added by syringe through a septum under a flow of nitrogen. The mixture was allowed to equilibrate at the reaction temperature of 25−60 °C for 10 min. Hydrogen peroxide (4000 μmol) was added by micropipet to the rapidly stirring solution. For adamantane oxidation, 15 mL of acetonitrile was used as a solvent. The samplings were carried out after 0.17, 0.5, 1, 2, 3, 24, 48, 72, 96, and 144 h. The reaction solution was analyzed by gas chromatograph (GC) and assignments were made by comparison with authentic samples analyzed under the same conditions.

Results and Discussion

Synthesis and X-ray Crystal Structure of $Fe[OSi(O^tBu)_3]_3$(THF). For attempts to produce well-defined iron centers supported on silica, we initially targeted an iron(III) molecular precursor supported by the $-OSi(O^tBu)_3$ ligand. Previously, the iron(III) siloxide complexes $[Fe(OSiR_3)_3]_2$ (R = Me, Et) were prepared by Schmidbaur and Richter.[52] These complexes must be handled at low temperatures, since they are thermally unstable with respect to elimination of the hexaalkyl disiloxide.

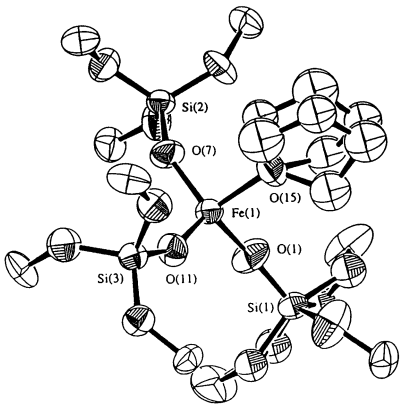

Figure 1. ORTEP drawing of $Fe[OSi(O^tBu)_3]_3$(THF). Methyl groups are omitted for clarity. The carbon atoms of the THF ligand and two oxygen atoms on Si(2) were modeled as distorted over two sites with equal populations.

Table 3. Selected Interatomic Distances (Å) and Angles (deg) for $Fe[OSi(O^tBu)_3]_3$(THF)

Bond Distances			
Fe(1)−O(1)	1.795(6)	Fe(1)−O(7)	1.814(6)
Fe(1)−O(11)	1.814(6)	Fe(1)−O(15)	1.994(7)
Si(1)−O(1)	1.568(6)	Si(2)−O(7)	1.576(6)
Si(3)−O(11)	1.571(7)		
Bond Angles			
O(1)−Fe(1)−O(7)	116.6(3)	O(1)−Fe(1)−O(11)	115.3(3)
O(1)−Fe(1)−O(15)	102.1(3)	O(7)−Fe(1)−O(11)	114.1(3)
O(7)−Fe(1)−O(15)	103.3(3)	O(11)−Fe(1)−O(15)	102.6(3)
Fe(1)−O(1)−Si(1)	157.9(5)	Fe(1)−O(7)−Si(2)	151.2(4)
Fe(1)−O(11)−Si(3)	156.2(4)		

The reaction between $FeCl_3$ and 3 equiv of $NaOSi(O^tBu)_3$ in refluxing THF for 12 h produced a light brown mixture. After three recrystallizations from pentane, pale yellow crystals of $Fe[OSi(O^tBu)_3]_3$(THF) were isolated in 74% yield (eq 1).

$$FeCl_3 + 3\ NaSi(O^tBu)_3 \xrightarrow[-3NaCl]{THF} Fe[OSi(O^tBu)_3]_3(THF) \quad (1)$$

A single-crystal structural analysis of $Fe[OSi(O^tBu)_3]_3$(THF) shows that this complex is monomeric (Figure 1). Bond distances and angles are listed in Table 3. The asymmetric unit contains two independent molecules, with the iron atom coordinated by three siloxide ligands and one THF molecule. The Fe−O bond lengths involving the siloxide ligands range from 1.795(6) to 1.814(6) Å, and these distances are in agreement with comparable Fe−O bond lengths in four-coordinate Fe(III) complexes[53−57] (these cover a wide range but average to ca. 1.86 Å[57]). As expected, the Fe−O bond length involving the datively bound THF molecule is somewhat longer (1.994(7) Å). The O−Fe−O bond angles involving the siloxide ligands range from 116.6(3) to 114.1(3)°, and the O−Fe−O bond angles range from 102.1(3) to 103.3(3)°. These values are also consistent with those observed for 4-coordinate $Fe^{III}O_4$

(52) Schmidbaur, H.; Richter, W. *Chem. Ber.* **1974**, *107*, 2427−2433.
(53) Le Maguerès, P.; Ouahab, L.; Golhen, S.; Grandjean, D.; Peña, O.; Jegaden, J.-C.; Gomez-Garcia, C. J.; Delhaès, P. *Inorg. Chem.* **1994**, *33*, 5180−5187.
(54) Bino, A.; Ardon, M.; Lee, D.; Spingler, B.; Lippard, S. J. *J. Am. Chem. Soc.* **2002**, *124*, 4578−4579.
(55) O'Keefe, B. J.; Monnier, S. M.; Hillmyer, M. A.; Tolman, W. B. *J. Am. Chem. Soc.* **2001**, *123*, 339−340.
(56) Marlin, D. S.; Olmstead, M. M.; Marscharak, P. K. *Inorg. Chim. Acta* **2000**, *294*, 106−114.
(57) Koch, S. A.; Millar, M. *J. Am. Chem. Soc.* **1982**, *104*, 5255−5257.

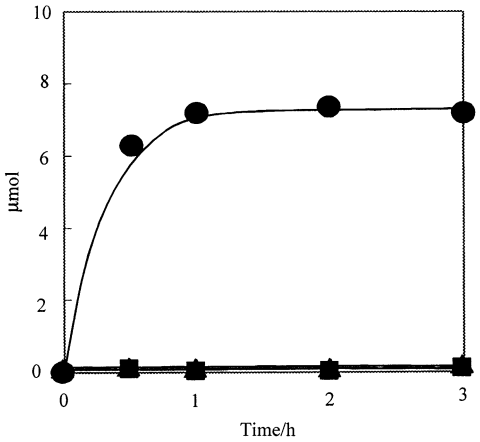

Figure 2. Time course for the grafting reaction of $Fe[OSi(O^tBu)_3]_3(THF)$ onto SBA-15. $HOSi(O^tBu)_3$, (●), HO^tBu, (▲), and THF, (■). Reaction conditions: $Fe[OSi(O^tBu)_3]_3(THF)$ 23 μmol, SBA-15 25 mg, and ferrocene 13 μmol. Reaction temperature 25 °C.

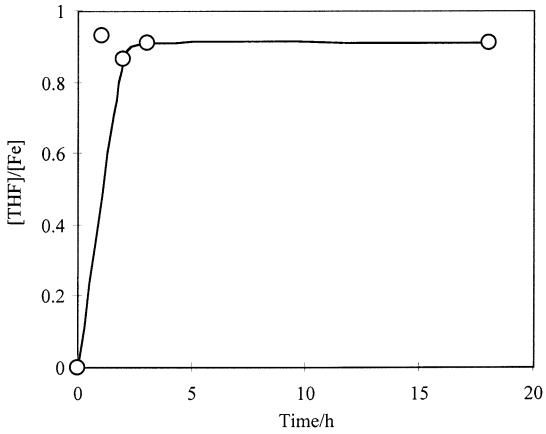

Figure 3. Time course for a ligand-exchange reaction of THF in 1.90% Fe/SBA-15 with CH_3CN, illustrating the THF/Fe molar ratio as a function of time. Reaction conditions: 1.90% Fe/SBA-15 (20 mg) and acetonitrile (0.04 g; 144 equiv/Fe). Reaction temperature 25 °C.

environments.[53−57] Thus, the coordination geometry of the Fe may be described as being slightly distorted from a tetrahedron, toward a trigonal pyramid. This distortion appears to result from the presence of three sterically demanding siloxide ligands. None of the oxygen atoms of the O^{t}Bu groups coordinate to the metal center, as is the case for the solid-state structures of some transition metal tris(*tert*-butoxyl)siloxy complexes.[40,41]

Grafting of $Fe[OSi(O^tBu)_3]_3(THF)$ onto SBA-15. The grafting of $Fe[OSi(O^tBu)_3]_3(THF)$ onto silica was accomplished by stirring a hexane solution of the precursor with the suspended support at room temperature for 24 h. Any unreacted iron precursor, and byproducts from the grafting reaction, were removed by washing the resulting solid with hexane.

The chemical reactions associated with the grafting process were monitored by ^{1}H NMR spectroscopy with benzene-d_6 as the solvent and ferrocene as an added standard. The precursor $Fe[OSi(O^tBu)_3]_3(THF)$ was not observed in this experiment due to its paramagnetic character. As the grafting reaction proceeded at room temperature, the elimination product $HOSi(O^tBu)_3$ was observed to form over a period of ca. 1 h, after which the SBA-15 surface appeared to be saturated (Figure 2). Note that THF and HO^tBu were not observed as elimination products over a period of 3 h. These results indicate that the grafting process involves only one type of reaction—the cleavage of an Fe−O bond of the precursor —and that the grafted iron species retain a THF ligand. The latter possibility is further supported by an experiment designed to displace this surface-bound THF ligand so that it could be observed by NMR spectroscopy. Thus, a freshly prepared sample of 1.90% Fe/SBA-15 (shown to contain 1.90 wt % iron by elemental analysis) was suspended in benzene-d_6, and to this suspension was added an excess of acetonitrile (144 equiv CH_3CN per Fe). The resulting ligand-exchange process occurred over ca. 3 h, to produce 0.91 equiv of free THF (per iron; see Figure 3). This result indicates that approximately every surface-bound iron center possesses one THF ligand.

The data described above are consistent with formation of structures involving one (**I**), two (**II**), or three (**III**) bonding interactions between the silica surface and each iron center (Scheme 2). A comparison of the measured maximum iron loading with the maximum amount of $HOSi(O^tBu)_3$ formed during the grafting process provides some evidence for the

Scheme 2

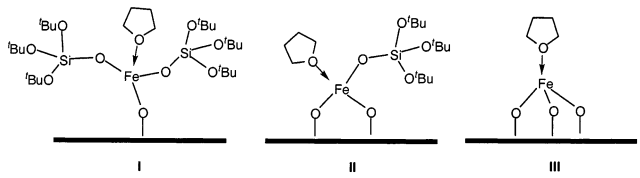

Table 4. C and H Elemental Analysis Results for 0.50 % and 1.90 %Fe-Grafted SBA-15

sample	possible structures	theoretical values of C and H (%)	obsd C and H elemental anal. (%)
0.50% Fe	Type I	C; 3.00, H; 0.55	C; 3.14, H; 0.52
	Type II	C; 1.72, H; 0.32	
	Type III	C; 0.43, H; 0.07	
1.90% Fe	Type I	C; 11.4, H; 2.09	C; 10.9, H; 1.89
	Type II	C; 6.54; H; 1.22	
	Type III	C; 1.63, H; 0.27	

predominant structure for the grafted iron species. By elemental analysis, the iron loading of an SBA-15 sample that had been treated exhaustively with an excess of iron precursor was 1.90%. Assuming structure **I**, the expected iron loading based on the amount of $HOSi(O^tBu)_3$ formed is 1.65%. This can be compared to the predicted iron loading based on structures **II** (0.83%) and **III** (0.55%). On the basis of these comparisons, we conclude that the structure of the surface-bound iron species is well represented by **I**. In addition, for grafted samples with 0.50 and 1.90 wt % Fe, the measured amounts of carbon and hydrogen (Table 4) are most consistent with a structure of type **I**, $\equiv SiO-Fe[OSi(O^tBu)_3]_2(THF)$.

An additional probe of the structure of the surface-bound iron species was based on UV−vis spectroscopy. For this purpose, the complex $Fe[OSi(O^tBu)_3]_3(THF)$ is expected to provide an excellent spectroscopic model for pseudotetrahedral iron centers bound to a THF ligand and three $-OSiO_3$ moieties (provided by the silica surface or the $OSi(O^tBu)_3$ ligand).[43,58] Figure 4 presents DRUV−vis spectra of $Fe[OSi(O^tBu)_3]_3(THF)$ and 0.35−1.90% Fe/SBA-15 samples before and after calcination (at 300 °C for 2 h under oxygen). The spectrum of solid $Fe[OSi(O^tBu)_3]_3(THF)$ is dominated by an intense band at

(58) Male, J. L.; Niessen, H. G.; Bell, A. T.; Tilley, T. D. *J. Catal.* **2000**, *194*, 431−444.

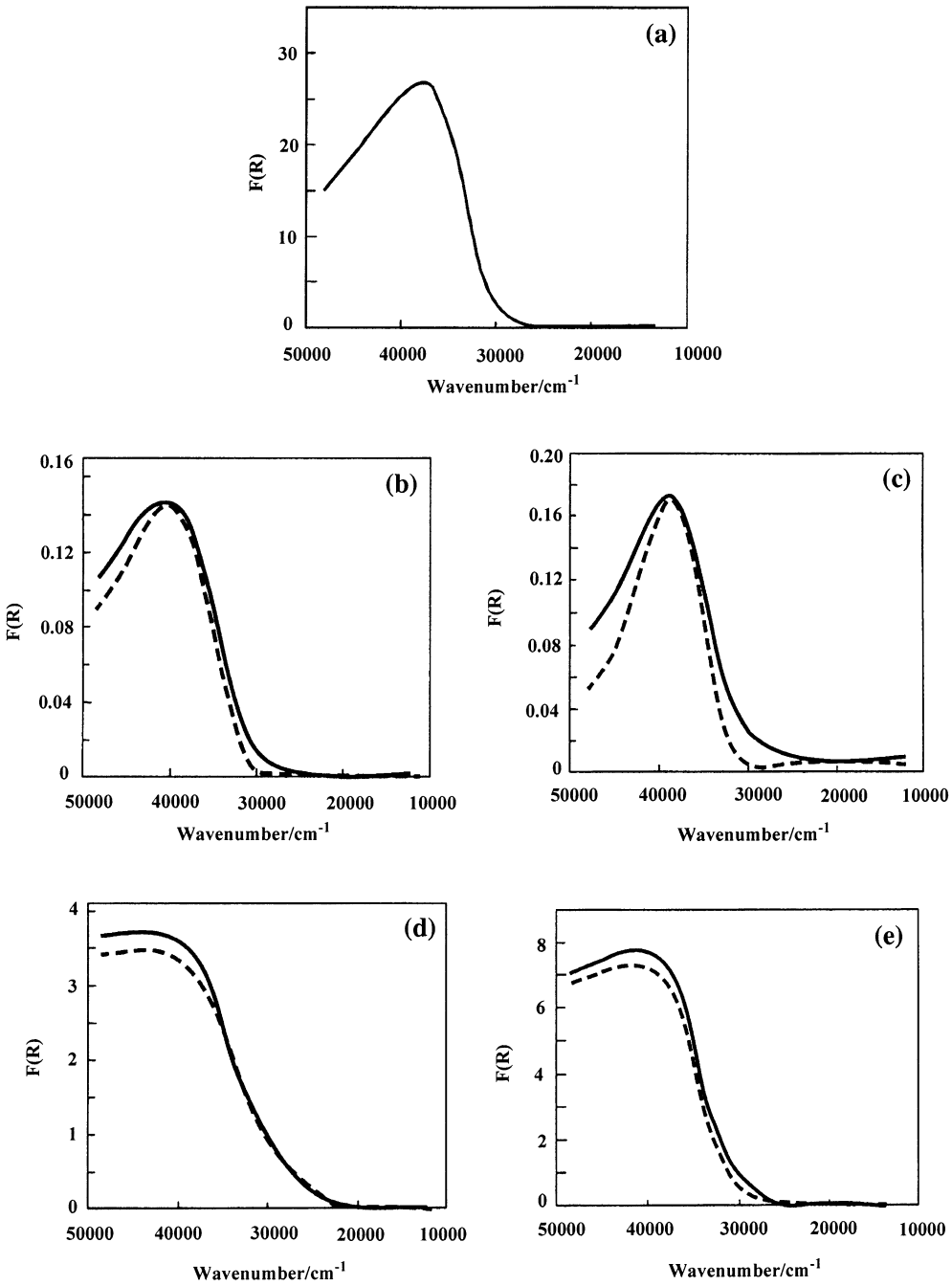

Figure 4. UV-vis spectra of (a) *as-prepared* Fe[OSi(O^{t}Bu)$_3$]$_3$(THF), (b) 0.35%, (c) 0.50%, (d) 1.33%, and (e) 1.90% Fe/SBA-15 before (—) and after (- - -) calcination.

38 310 cm^{-1} (Figure 4a). This absorption is attributed to a charge-transfer (CT) band, as these are typically observed for Fe^{3+} species in the range of 30 000−50 000 cm^{-1}.[59−61] In hexane solution, the UV−vis spectrum of Fe[OSi(O^{t}Bu)$_3$]$_3$(THF) exhibits a CT band at ca. 37 594 cm^{-1} (ϵ = 23 88 M^{-1} cm^{-1}). A very broad band assigned as a *d*−*d* transition for high-spin Fe^{3+} was also observed at ca. 22 124 cm^{-1} (ϵ = 11 M^{-1} cm^{-1}; in hexane).[60]

At low loadings of the iron species onto SBA-15, the spectra are very similar to those of Fe[OSi(O^{t}Bu)$_3$]$_3$(THF), with observed bands appearing at 40 965, 40 695, and 39 495 cm^{-1} for the 0.056, 0.35, and 0.50 wt % Fe/SBA-15 samples, respectively (parts b−d of Figure 4). These band positions are quite different from those observed for FeZSM-5 (42 735 and 77 170 cm^{-1})[59] and Fe-silicalite (41 500 and 46 500 cm^{-1}),[60] but this is not too surprising given the apparent Fe[OSiO$_3$]$_3$-(THF) coordination environment for the Fe/SBA-15 samples. Further comparisons can be made with the reported positions of CT bands for isolated Fe^{3+} species in octahedral complexes (ca. 36 000 cm^{-1}) and octahedral Fe^{3+} in small clusters (ca. 30 000 cm^{-1}).[60] Thus, the UV−vis spectra make it possible to rule out the presence of iron oxide clusters in our samples, but we cannot at this time exclude the presence of small amounts of octahedral Fe^{3+}.

(59) Ribera, A.; Arends, I. W. C. E.; de Vries, S.; P.-Pamírez, J.; Sheldon, R. A. *J. Catal.* **2000**, *195*, 287−297.
(60) Bordiga, S.; Buzzoni, R.; Geobaldo, F.; Lamberti, C.; Giamello, E.; Zecchira, A.; Leofanti, G.; Petrini, G.; Tozzola, G.; Vlaic, G. *J. Catal.* **1996**, *158*, 486-501.
(61) Tippins, H. H. *Phys. Rev. B* **1970**, *1*, 126−135.

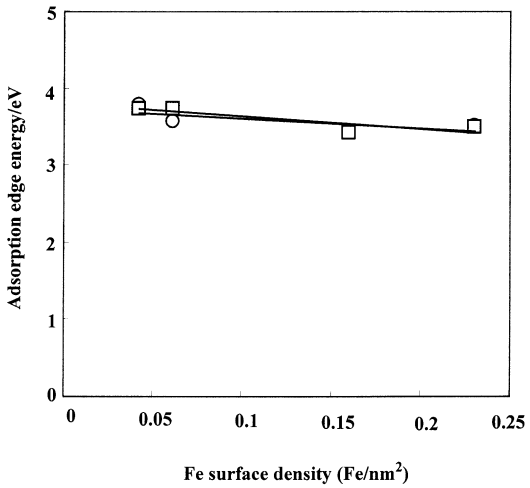

Figure 5. Effect of Fe surface density on absorption edge energies for silica-supported iron species (a) before (□) and (b) after (○) calcination.

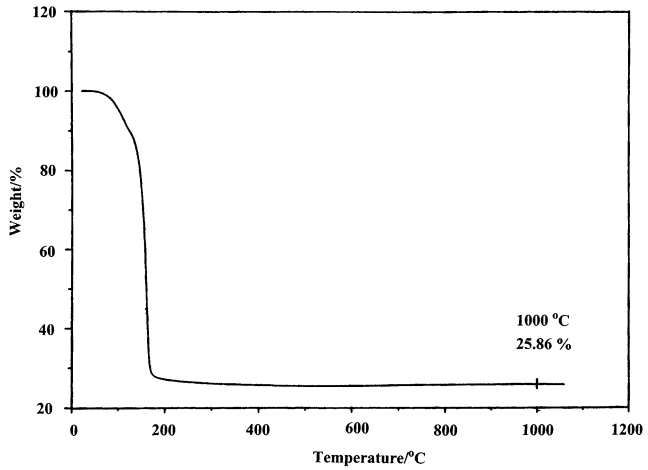

Figure 6. TGA trace for Fe[OSi(O^{t}Bu)$_3$]$_3$(THF) under N_2, with a heating ratio of 10 °C min^{-1}.

At higher Fe loadings (1.33 and 1.90 wt %), the UV−vis absorption maxima were close to those observed for samples with a lower loading, but in these cases the bands were broader, and it was difficult to define a precise position for these bands from the energy at maximum absorption. In such cases, absorption edge energies sometimes provide a more convenient description of the electronic properties of the solid. The absorption edge energies for all the UV−vis spectra were determined using Tauc's law, an expression that describes the near-edge region of an absorption in semiconductors with indirect band-gap transitions.[62] Using this expression, the edge energy is obtained from the intercept of a straight line fitted through the rise of the function $[F(R_\infty)h\nu]^{1/2}$ plotted versus $h\nu$,[63] where $F(R_\infty)$ is the Kubelka−Munk function[64] and $h\nu$ is the energy of the incident photon. The position of the adsorption-edge energy for low-energy charge-transfer transitions has been shown to correlate with the domain size of semiconductors and insulators.[65−71] The energy at the absorption edge has been recently used to characterize the size of MoO_x,[70] WO_x,[63] and VO_x[72] domains in catalytic solids, in which the absorption edge energies decreased dramatically with increasing metal surface densities. The changes in absorption edge energies as a function of Fe surface density is illustrated in Figure 5a. These data indicate that there is not a significant change in the structure of the surface-bound iron species as the Fe surface density increases.

Calcination of the Iron-Grafted SBA-15 Materials. The surface-bound ≡SiO−Fe[OSi(O^{t}Bu)$_3$]$_2$(THF) species was expected to cleanly decompose thermally at low temperature, and this was indicated by the thermal gravimetric analysis (TGA) of Fe[OSi(O^{t}Bu)$_3$]$_3$(THF). The TGA curve of Fe[OSi(O^{t}Bu)$_3$]$_3$-(THF) heated under flowing N_2 is shown in Figure 6. A gradual weight loss begins at 50 °C and is followed by a precipitous weight loss with an onset temperature of ca. 140 °C. By 170 °C this weight loss is complete. The final ceramic yield at 1000 °C is 25.9% under N_2. For comparison, a ceramic yield of 30.7% would correspond to formation of $^1/_2Fe_2O_3{\cdot}3SiO_2$.

Calcinations of the iron-grafted SBA-15 materials were carried out by heating the samples at 300 °C for 2 h under oxygen. This treatment resulted in a dramatic reduction of the carbon and hydrogen contents for the 0.0−1.90% Fe/SBA-15 samples, to levels of 0.3−0.5% for carbon and 0.4−0.7% for hydrogen. UV−vis spectra of these materials indicate that there is little change in the coordination environment of the iron upon calcination. As shown in Figure 5, the calcined samples exhibit CT bands that are similar in energy and line width to those of the corresponding uncalcined samples. In addition, the absorption edge energies for the calcined samples do not decrease significantly with increasing Fe surface density (Figure 5b). This implies that the calcination process does not lead to condensation of the iron centers into iron oxide clusters. This is further suggested by the absence of CT bands attributed to Fe^{3+} species in octahedral complexes (at ca. 36 000 cm^{-1}) or small clusters (at ca. 30 000 cm^{-1}). On the basis of these observations, we conclude that (1) the iron species on the silica surface retain their isolated Fe^{3+} structure after calcination and (2) no iron oxide clusters are formed under the calcination conditions.

EPR spectroscopy has been used extensively to probe the local environment of Fe^{3+} centers incorporated into silicas and zeolites.[35,59,60,73] In this context, the precursor complex Fe[OSi-(O^{t}Bu)$_3$]$_3$(THF) offers an interesting and potentially useful model. Figure 7 presents the X-band EPR spectrum of this species, which contains signals at $g = 5.5$ and 2.0. This spectrum is consistent with what is expected for a four-coordinate, high-spin, Fe^{3+} ion in a C_{3v} environment, for which $g_\perp \approx 6$ and $g_{||} \approx 2$.[60,74] Figure 7 also shows the X-band EPR spectra of the grafted samples Fe/SBA-15, at 0.50 and 1.90 wt % loadings, before and after calcination. For all iron-grafted samples before

(62) Tauc, J. In *Amorphous and Liquid Semiconductors*; Tauc, J., Ed.; Plenum: London, 1974.
(63) Barton, D. G.; Shtein, M.; Wilson, R. D.; Soled, S. L.; Iglesia, E. *J. Phys. Chem. B* **1999**, *103*, 630−640.
(64) Delgass, W. N. In *Spectroscopy in Heterogeneous Catalysis*; Academic Press: New York, 1979.
(65) Cherstnoy, N.; Hull, R.; Brus, L. E. *J. Chem. Phys.* **1986**, *85*, 2237−2242.
(66) Alivisatos, A. P. *Science* **1996**, *271*, 933−937.
(67) Service, R. F. *Science* **1996**, *271*, 920−922.
(68) Hoener, C. F.; Allan, K. A.; Bard, A. J.; Campion, A.; Fox, M. A.; Mallouk, T. E.; Webber, S. E.; White, J. M. *J. Phys. Chem.* **1992**, *96*, 3812−3817.
(69) Brus, L. *J. Phys. Chem.* **1986**, *90*, 2555−2560.
(70) Weber, R. S. *J. Catal.* **1995**, *151*, 470−474.
(71) Fournier, M.; Louis, C.; Che, M.; Chaquin, P.; Masure, D. *J. Catal.* **1989**, *119*, 400−414.
(72) Khodakov, A.; Yang, J.; Su, S.; Iglesia, E.; Bell, A. T. *J. Catal.* **1998**, *177*, 343−351.
(73) Goldfarb, D.; Bernard, M.; Strohmainer, K. G.; Vaughan, D. E. W.; Thomann, H. *J. Am. Chem. Soc.* **1994**, *116*, 6344−6353.
(74) Lin, D. H.; Coudurier, G.; Vedrine, J. C. *Stud. Surf. Sci. Catal.* **1989**, *49*, 1431−1448.

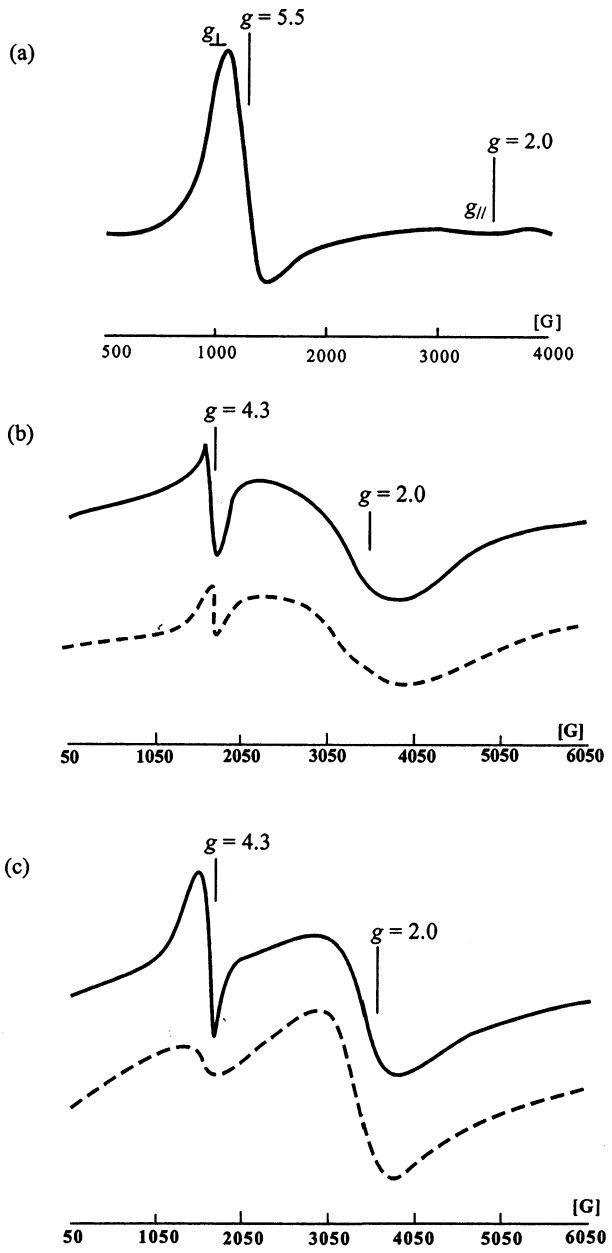

Figure 7. EPR spectra of (a) as-prepared Fe[OSi(O^{t}Bu)$_3$]$_3$(THF), (b) 0.50%, and (c) 1.90% Fe/SBA-15 before (—) and after (- - -) calcination.

and after calcination, the spectra display signals with g values of 4.3 and 2.0. This indicates that the coordination environment of the grafted iron species is at least somewhat different from that of the precursor complex. Such signals have often been observed for isolated iron centers incorporated into silicas[60,73] and zeolites (e.g., for FeHZSM-5[59]), and may be attributed to high-spin Fe^{3+} in a distorted tetrahedral environment. Note, however, that the signal at $g = 2.0$ may also indicate some contribution from undistorted tetrahedral or octahedral Fe^{3+} sites.[73] There is no evidence for iron oxide clusters in these samples, as these are expected to exhibit g values of 2.2−2.5.[73,75,76] From these observations, it is possible to conclude that the iron sites in the grafted samples prepared in this study

Scheme 3

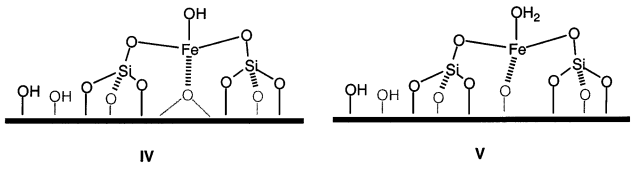

(whether calcined or not) possess isolated Fe^{3+} centers. These Fe^{3+} centers appear to have a similar, distorted tetrahedral structure that persists over a range of iron loadings and after calcination to 300 °C under oxygen. Although we cannot currently assign a specific structure to these species, the postulated structures **IV** and **V** in Scheme 3 are consistent with the available data.

Calcination of the Fe/SBA-15 samples was monitored by in situ IR spectra. Before calcination, the 1.90% Fe/SBA-15 sample exhibited the expected C−H vibrational bands, at 2848, 2913, 2960, and 2984 cm^{-1}.[77] As the temperature of the sample was raised from 25 to 500 °C, these bands diminished in intensity. Most of the bands were absent from the spectra at 225 °C, and by 375 °C there was no evidence for C−H bands. These results correspond to the complete removal of the −O^{t}Bu and THF ligands from the grafted molecular species during heat treatment.

Catalytic Oxidations. The Fe-grafted SBA-15 materials were examined as catalysts for various hydrocarbon oxidation reactions, as summarized in Table 5. For these studies, only materials that had been calcined (at 300 °C for 2 h under oxygen) were employed. In each case, the oxidant was hydrogen peroxide.

The oxidation of benzene at 60 °C, as catalyzed by 0.50% Fe/SBA-15, was monitored by gas chromatography. The conversion to phenol was highly selective (ca. 100% after 96 h and 145 turnovers; this corresponded to 42% conversion of hydrogen peroxide and 7.5% conversion of benzene) and occurred with a turnover frequency (TOF = (mol of products/mol of Fe in catalyst) s^{-1}) of 2.5×10^{-3} s^{-1} (calculated after a reaction time of 1 h). No induction period was observed for this reaction (≥10 min). Thus, no products resulting from the formation of phenyl radicals[78] (e.g., biphenyl, *p*-benzoquinone, and catechol) were observed, even after 96 h. For comparison, Fenton's reagent (which appears to operate via a radical process) gives conversions to phenol (88%) and biphenyl (12%) under comparable conditions.[78] The observed TOF compares favorably with those reported for other heterogeneous systems involving supported iron. For example, silica impregnated with $FeCl_3$ has been reported to catalyze the oxidation of benzene by hydrogen peroxide with a TOF of 5.9×10^{-3} s^{-1}; however the selectivity was only 77%.[15,79] In addition, TOFs for this reaction have been reported for $FeCl_3/Al_2O_3$ (6.1×10^{-4} s^{-1}), $FeCl_3$/silica−alumina (4.4×10^{-4} s^{-1}), and $FeCl_3/TiO_2$ (3.0×10^{-4} s^{-1}).[79]

Earlier work on the mechanism of iron-catalyzed oxidations with H_2O_2 has addressed the possible intermediacy of radical species (•OH or •R).[80] For example, it has been found that radical-based oxidations in acetone solvent proceed much more slowly than in acetonitrile, since acetone is an effective trap for •OH.[81] Thus, the effect of acetone solvent in the benzene

(75) Wechuysen, B. M.; Wang, D.; Rosynek, M. P. R.; Lunsford, J. H. *Angew. Chem., Int. Ed. Engl.* **1997**, *36*, 2374−2376.
(76) Selvam, P.; Dapurkar, S. E.; Badamali, S. K.; Murugasam, M.; Kuwano, H. *Catal. Today* **2001**, *68*, 69−74.
(77) Silverstein, R. M.; Bassler, G. C.; Morrill, T. C. In *Spectrometric Identification of Organic Compounds*, 5th ed.; John Wiley & Sons: New York, 1991.
(78) Walling, C.; Johnson, R. A. *J. Am. Chem. Soc.* **1975**, *97*, 363−367.
(79) Seo, Y.-J.; Tagawa, T.; Goto, S. *J. Chem. Eng. Jpn.* **1994**, *27*, 307−308.
(80) Arends, I. W. C. E.; Ingold, K. U.; Wayner, D. D. M. *J. Am. Chem. Soc.* **1995**, *117*, 4710−4711.

Table 5. Oxidation of Various Substrates Catalyzed by 0.50 and 1.90 % Fe-Grafted SBA-15 with Hydrogen Peroxide[a]

substrate (mmol)	Fe wt %	reaction temp (°C)	product (selectivity %)[b]	TOF[c]
benzene (22.4)	0.50	60	phenol (100)	2.5×10^{-3}
toluene (22.4)	1.90	60	*o*-cresol (35) *m*-cresol (0) *p*-cresol (33) benzaldehyde (32)	5.5×10^{-4}
cyclohexene (18.5)	1.90	25	cyclohexene oxide (45) cyclohexen-1-ol (22) cyclohexen-1-one (33)	1.8×10^{-2}
cyclooctene (18.5)	0.50	25	cyclooctene oxide (99) cycloocten-1-ol (1) cycloocten-1-one (0)	6.2×10^{-4}
cyclohexane (18.5)	0.50	60	cyclohexanol (100) (68)[d] cyclohexanone (0) (32)[d]	7.2×10^{-6} (1.2×10^{-4})[d]
adamantane (22.4)	0.50	60	1-adamantanol (55) 2-adamanatanol (27) 2-adamanatnone (18) (3 °/2° = 3.7)	1.2×10^{-3}
benzyl alcohol (22.4)	0.50	60	benzaldehyde (100)	1.2×10^{-2}

[a] Reaction conditions: Substrates 18.5−22.4 mmol, catalyst 130 mg, H_2O_2 4000 μmol, CH_3CN 5 mL, reaction time 24−144 h, reaction temperature 25−60 °C, dodecane (internal standard) 428 μmol. [b] After 1 h. [c] TOF = TON ((mol product)/(mol Fe)) s^{-1} after 1 h. [d] After 144 h.

oxidation described above was investigated. At 25 °C in acetone, the TOF for the oxidation of benzene to phenol by 1.90% Fe/SBA-15 was 3.3×10^{-5} s^{-1}. Under the same conditions, this oxidation in acetonitrile proceeded with a TOF of 5.4×10^{-5} s^{-1}. The similarity of these results suggests that the oxidation occurs mainly via a nonradical pathway.

The 1.90% Fe/SBA-15 material was observed to catalyze the oxidation of toluene to a mixture of benzaldehyde (32%) and *o*- and *p*-cresol (68%). Note that Fenton's reagent also gives these products, in addition to benzyl alcohol and bibenzyl.[78] To our knowledge, there are no literature reports on related toluene oxidations by heterogeneous Fe/SiO_2 catalysts, but various homogeneous iron systems exhibit lower TOFs and give lower conversions to cresols.[82,83]

To determine whether the active species leached into solution during a typical catalytic run, a sample of 1.90% Fe/SBA-15 and H_2O_2 in acetonitrile was heated to 60 °C for 3 h with rapid stirring. The mixture was then filtered while still hot and the filtrate was treated with toluene at 60 °C.[84] Samples of this reaction mixture taken after 1, 2, and 3 h contained no oxidized products, indicating that the observed catalysis was heterogeneous. In addition, the solid obtained from the filtration was observed to catalyze the oxidation of toluene at 60 °C. The TOF for this second run (2.6×10^{-4} s^{-1}) was slightly lower than that of the first (5.5×10^{-4} s^{-1}), indicating a small amount of degradation of the catalyst.

Figure 8 presents data that illustrate the dependence of catalytic activity (for the oxidation of toluene at 60 °C) on the degree of iron loading. These results, which indicate very little change in activity as a function of iron coverage, are consistent with the presence of isolated iron sites over a rather wide range of loadings. This is consistent with spectroscopic data (vide supra) that suggest that these iron sites possess the same, or very similar, structures.

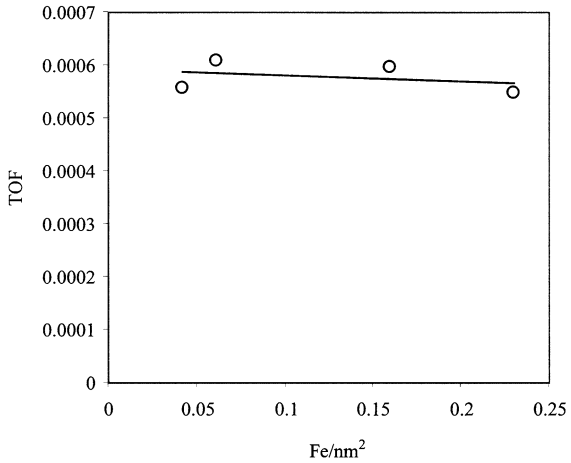

Figure 8. Dependence of TOF on Fe surface density for toluene oxidation with hydrogen peroxide at 60 °C.

For the oxidation of toluene at 25 °C, we also investigated the influence of catalyst calcination temperature on catalyst activity of 1.90% Fe/SBA-15. For the uncalcined catalyst, the TOF (3.6×10^{-4} s^{-1}) was highest, and a slight decrease in activity was observed upon calcination to 200 (3.1×10^{-4} s^{-1}) and 300 °C (3.1×10^{-4} s^{-1}). However, after heat treatment at 500 °C for 10 h under oxygen, the catalyst activity decreased dramatically. Consistent with this observation, the DRUV−vis spectrum of 1.90% Fe/SBA-15 calcined at 500 °C exhibited a weak CT band associated with isolated iron (at ca. 40 000 cm^{-1}) and a significant absorption at ca. 30 000 cm^{-1}, indicating the presence of iron oxide clusters.[60]

The oxidation of cyclohexane to cyclohexanol at 60 °C (with 1.90% Fe/SBA-15 catalyst) proceeded with high selectivity (ca. 100%) over 24 h, but at a low rate (7.2×10^{-6} s^{-1} calculated at 24 h; only 0.7 turnovers). After 24 h, cyclohexanone was observed as a new product, and its concentration increased with time, reaching a yield of 32% after 144 h. Interestingly, in this second phase of the reaction, the TOFs for cyclohexanone (3.8×10^{-5} s^{-1}) and cyclohexanol (8.2×10^{-5} s^{-1}) production reflect the presence of a more active catalyst. The observed change in selectivity may reflect the formation of O_2, which could propagate a radical chain process.[80] For an MCM-41 catalyst that was grafted with iron via 3-aminopropyltrimethoxy-

(81) Roelfes, G.; Lubben, M.; Hage, R.; Que, L., Jr.; Feringa, B. L. *Chem. Eur. J.* **2000**, *6*, 2152−2159.
(82) Brook, A. M.; Castle, L.; Smith, J. R. L.; Higgins, R.; Morris, K. P. *J. Chem. Soc., Perkin Trans. 2* **1982**, 687−692.
(83) Fish, R. H.; Koggins, M. S.; Oberhausen, K. J.; Fong, R. H.; Yu, W. M.; Christou, G.; Vincent, J. B.; Coggin, D. K.; Buchanan, R. M. *Inorg. Chem.* **1991**, *30*, 3002−3006.
(84) Sheldon, R. A.; Wallau, M.; Arends, I. W. C. E.; Schuchardt, U. *Acc. Chem. Res.* **1998**, *31*, 485−493.

silane, the TOF calculated at 144 h was 1.6×10^{-4} s^{-1}. In this case, the cyclohexanol/cyclohexanone ratio of 1 indicates the operation of a radical-based mechanism.[35]

For the oxidation of cyclohexane, the kinetic isotope effect may indicate the operation of radical-based mechanisms.[81] More specifically, a k_H/k_D value in the range of 1−2 is thought to reflect a radical chain autoxidation mediated by •OH.[85] For the system described here, the k_H/k_D ratio for the formation of cyclohexanol was determined in competition experiments between the oxidations of cyclohexane and cyclohexane-d_{12}, catalyzed by 1.90% Fe/SBA-15 at 60 °C in acetonitrile. The observed value of 2.6 for k_H/k_D would seem to indicate a nonradical process. However, iron porphyrin catalysts that appear to operate via hydrogen abstraction by an iron−oxo (Fe═O) intermediate exhibit k_H/k_D values of ≥ 10.[86]

For the oxidation of cyclohexene, the observed products (cyclohexene oxide, cyclohexen-1-ol, and cyclohexen-1-one) reflect a low selectivity for the activation of allylic C−H bonds.[81] These results, along with those described above, suggest that the Fe/SBA-15 catalysts operate primarily via nonradical processes. A similar selectivity was reported for an Fe/SiO_2 catalyst prepared by ion beam implantation, which produced cyclohexene oxide in 49% yield. The latter catalyst, however, exhibited a lower TOF (5.8×10^{-3} s^{-1}) than that observed for 1.90% Fe/SBA-15 (1.8×10^{-2} s^{-1}).[87] Note that the epoxidation of cyclooctene occurs with a high degree of selectivity (99% out to 131 turnovers; Table 5). For comparison, the selective iron epoxidation catalyst recently reported by Jacobsen gives a selectivity for cyclooctene epoxidation of 86%.[31]

Adamantane is an interesting substrate for catalyzed oxidations, since the ratio of products resulting from reactions at the secondary and tertiary postions can reflect the radical nature of the oxidation mechanism.[81] For the 0.50% Fe/SBA-15 catalyst, oxidation occurred at both the secondary and tertiary carbon centers of adamantane (TOF = 1.2×10^{-3} s^{-1}), with an observed 3°/2° ratio, normalized on a per-hydrogen basis, of 3.7. This ratio is different from that expected for a radical process (ca. 2).[88]

Concluding Remarks

The covalent attachment of molecular species onto the surface of silica, via elimination reactions involving surface-bound hydroxyl groups, is a commonly employed method for the synthesis of heterogeneous catalysts that contain transition metal active sites.[89] Both organometallic[90,91] and inorganic[89] species have been introduced in this manner, but it seems generally more difficult to control the structures of catalytic sites introduced with simple inorganic salts (e.g., a metal halide). This difficulty relates to the tendency of inorganic species to condense, particularly under aqueous conditions.[7] In this contribution, we have employed a new approach for the introduction of inorganic surface sites of controlled structure.[46,47] This method features a molecular precursor approach which allows generation of stable, single-iron sites supported on silica (SBA-15). Previous attempts to introduce such species in a controlled manner have been complicated by the hydrolysis and migration of iron species, which lead to iron clusters upon heat treatment of the catalyst.

The grafting chemistry involving the molecular precursor $Fe[OSi(O^tBu)_3]_3(THF)$ is quite clean, such that upon reaction with the hydroxylated silica surface of SBA-15, one siloxide ligand is eliminated as $HOSi(O^tBu)_3$ to give a mononuclear iron(III) species of the type $\equiv Si-O-Fe-[OSi(O^tBu)_3]_2(THF)$ (**I**). Remarkably, the calcination of this species at 300 °C cleanly removes the organic groups of the grafted species to produce a thermally stable, isolated mononuclear iron(III) structure. Several factors appear to be important in the successful generation of these stable sites. For example, the remaining siloxide ligands of the grafted molecular species contribute additional SiO_4 units to the surface upon calcination, and these may help stabilize the mononuclear inorganic iron center. The use of hydrophobic solvents for the grafting procedure ensures that competing hydrolysis and condensation of the iron centers does not occur. Finally, the relatively low OH coverage for SBA-15 (1.0 nm^{-2}) and the high dispersity of the iron surface species on the silica surface may help suppress condensation processes. This work appears to support the view that designed chemical reactions of molecular species on a solid surface offer considerable potential for generating catalytic sites with targeted structures.[47,90−93]

There has been considerable interest in the use of iron-based catalysts for the selective oxidation of hydrocarbons. For many of these catalysts, the combination of an iron species with hydrogen peroxide gives rise to Harber−Weiss chemistry, generating hydroxyl radicals that initiate radical autoxidation reactions.[80] However, the heterogeneous system described here appears to operate via nonradical processes. Although the exact nature of the active species is still undefined, it seems clear that the Fe/SBA-15 catalysts described here exhibit high selectivities in various hydrocarbon oxidations, with TOFs that compare favorably with those reported for related heterogeneous systems. The catalytic observations appear to be strongly associated with isolated, pseudotetrahedral Fe(III) sites supported by silica. Thus, the Fe/SBA-15 catalysts will serve as an important basis for comparison as structure−reactivity relations are developed. Future efforts will involve the use of molecular precursor routes to obtain supported iron catalysts in which the structure of the iron center, and the support, are varied.

Acknowledgment. This work was supported by the Director, Office of Energy Research, Office of Basic Energy Sciences, Chemical Sciences Division, of the U.S. Department of Energy under Contract No. DE-AC03-76SF00098. We gratefully acknowledge Mr. Benjamin R. Wood for in situ IR measurements.

Supporting Information Available: Crystallographic data (PDF). This material is available free of charge via the Internet at http://pubs.acs.org.

JA020388T

(85) Khenkin, A. M.; Shilov, A. E. *New J. Chem.* **1989**, *13*, 659−667.
(86) Meunier, B. *Chem. Rev.* **1992**, *92*, 1411−1456.
(87) Yang, Q.; Li, C.; Wang, S.; Lu, J.; Ying, P.; Xin, Q.; Shi, W. *Stud. Surf. Sci. Catal.* **2000**, *130*, 221−226.
(88) Singh, B.; Long, J. R.; de Biani, F. F.; Gatteschi, D.; Stavropoulos, P. *J. Am. Chem. Soc.* **1997**, *119*, 7030−7047.
(89) Smith, G. V.; Notheisz, F. In *Heterogeneous Catalysis in Organic Chemistry*; Academic Press: New York, 1999.
(90) Basset, J. M.; Scott, S. L.; Choplin, A.; Leconte, M.; Quignard, F.; Santini, C.; Thèolier, A. In *Elementary Reaction Steps in Heterogeneous Catalysis*; Joyner, R. W.; Santen, R. A. V., Eds.; Kluwer: Dordrecht, 1993; pp 39−49.
(91) Basset, J. M.; Gates, B. C.; Candy, J.-P.; Choplin, A.; Leconte, M.; Quignard, F.; Santini, C. In *Surface Organometallic Chemistry: Molecular Approaches to Surface Catalysis*; Kluwer: Dordrecht, 1988.
(92) Anwander, R. *Chem. Mater.* **2001**, *13*, 4419−4438.
(93) Arends, I. W. C. E.; Sheldon, R. A. *Appl. Catal. A* **2001**, *212*, 175−187.